# Elastocapillary filling of deformable nanochannels

J. W. van Honschoten,[a] M. Escalante, N. R. Tas, H. V. Jansen, and M. Elwenspoek
*MESA+ Institute for Nanotechnology, University of Twente, P.O. Box 217, 7500 AE Enschede, The Netherlands*

(Received 21 December 2006; accepted 15 March 2007; published online 15 May 2007)

The capillary filling speed of wetting liquids of varying viscosity and surface tension in hydrophilic nanochannels with an elastic capping layer has been analyzed. The channels, with a height just below 80 nm, are suspended by a thin flexible membrane that easily deforms due to the negative pressure which develops behind the moving meniscus. In the elastocapillary filling of the channels, two opposite effects compete: the decreased cross channel sections increase the flow resistance, while the Laplace pressure that acts as the driving force becomes more negative due to the increased meniscus curvature. Although the meniscus position shows a square root of time behavior as described by the Washburn relation, the net result of the induced bending of the membranes is a definite increase of the filling speed. We propose a relatively straightforward model for this elastocapillary process and present experimental results of the filling speed of ethanol, water, cyclohexane, and acetone that are found to be in good agreement with the presented model, for membrane deflections of up to 80% of the original channel height. © *2007 American Institute of Physics*. [DOI: 10.1063/1.2732539]

## I. INTRODUCTION

Nanochannels are defined as channels having at least one dimension on the order of 100 nm or smaller.[1–6] Due to the small dimensions, capillary action is very prominent in such channels and can lead to a negative absolute pressure.[7,8] The concept of capillary negative pressure is well appreciated in the field of geochemistry,[7] while deformable planar nanochannels offer a unique way for direct measurement of the negative pressures.[8] Sobolev *et al.*[9] measured the capillary pressure of water in quartz capillaries with radii ranging from 200 down to 40 nm, and showed that on the 100 nm length scale the Young-Laplace equation is still valid. Capillary filling experiments have been done on a larger scale (around 3 $\mu$m channel height),[10] revealing that the filling speed can qualitatively be described by the Washburn model.[11] The capillary filling speed in one-dimensional nanochannels with a height down to 50 nm was studied by Tas *et al.*[12] who found that the apparent viscosity of polar liquid with low ionic concentration such as de-ionized water in nanoconfinement is higher than its bulk value causing a lower than expected filling speed. This effect has been attributed to the electroviscous effect. Before this study, Churaev *et al.*[13] and Hibara *et al.*[14] suggested an essential difference of the viscosity on the nanoscale with respect to the bulk value. The filling kinetics of channels with even smaller cross section was also investigated, where Han *et al.*[15] studied capillaries with diameters down to 27 nm. The smallest nanochannels studied had heights down to 5 nm, recently fabricated by Haneveld,[16] who found a slightly increased viscosity in channels of 10 nm.

In the present study, silicon micromachining incorporating a thin membrane transfer technique to encapsulate trenches is used to create hydrophylic nanochannels. Such a thin deformable capping layer is a perfect candidate to characterize the elastocapillary effects related to the induced negative pressure in the fluid.

The capillary-driven coalescence of flexible structures, as it was observed in the tarsi of insects[17] and in biomimetic adhesives[18] is a prominent adhesion process that can have damaging effects in microelectromechanical structures[19–24] or carbon nanotubes,[24–26] but can also appear useful, in the assembly of small structures such as nanochannels[5] and other micro- and nanofabrication technologies, or, as suggested very lately, be used to produce three dimensional structures through the wrapping of a liquid droplet by an elastic sheet.[27] Elastocapillarity has only recently become a subject of specific investigation, especially in the context of the elastocapillary interaction between two long flexible sheets with a surface-tension-driven rise of a liquid in between, by Kim and Mahadevan[28] and the elastocapillary coalescence in wet hair.[29] These studies report on the sticking of two closely spaced lamellae[29] or sheets[28] placed vertically in a bath of wetting liquid where capillary suction bends the flexible structures and the liquid in between rises. However, these authors analyze the static equilibrium of elastocapillarity, when there is a balance between capillarity and elasticity, for length scales on the order of the Jurin length $l_J=2\gamma/\rho g r$ (with $\gamma$ and $\rho$ the liquid's surface tension and density, respectively, and $r$ the capillary radius) and where gravity plays a role. In this paper we concentrate on the time development of the phenomenon, in particular on the nanoscale, where gravity effects can be neglected. The capillary filling we observe results from the mutual interaction between the elastic deformation of the channels and the pressure distribution of the moving fluid. In this process two different effects related to the channel deformation compete: the decreased cross sections of the channel increase the flow resistance, while the Laplace pressure, acting as the driving force, becomes more

[a]Author to whom correspondence should be addressed; electronic mail: j.w.vanhonschoten@utwente.nl

 © 2007 American Institute of Physics

Downloaded 09 Jul 2007 to 130.89.1.19. Redistribution subject to AIP license or copyright, see http://jap.aip.org/jap/copyright.jsp

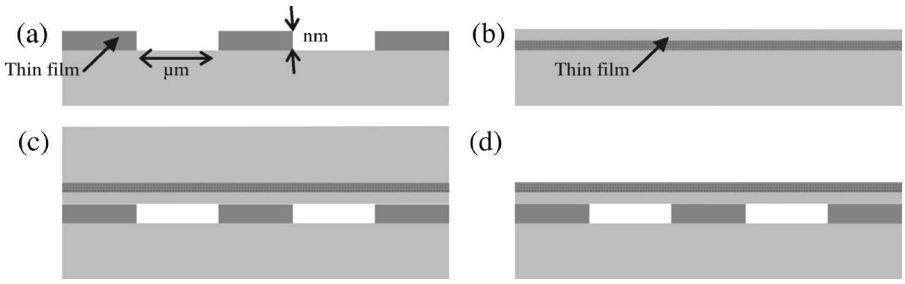


FIG. 1. Cross section. (a) Processed bottom wafer with oxide spacer layer. (b) Processed top wafer. (c) Bonded pair. (d) Removal of the wafer support to release the thin film.

negative as a result of the increased meniscus curvature. In this paper we show that the filling behavior follows the classical diffusive-type $x \sim t^{1/2}$ law, but that the net effect of these two opposite effects is an increase of the filling velocity compared with that in an undeformed rectangular channel.

In Sec. II is shortly described the fabrication of the hydrophylic nanochannels that are used for the investigation of the filling behavior. In Sec. III a model is presented for the capillary filling in these channels where the membranes bend downward due to the induced negative pressure. The results are compared with the classical Washburn law for filling in undeformable channels. Section IV presents the results of the filling experiments and relates these to the model. It shows that the experimental measurements are in good agreement with the model predictions.

## II. FABRICATION

We created arrays of hydrophilic channels of different widths in the micrometer range and height of about 80 nm with a capping layer consisting of a laminate of SiN and $SiO_2$. Access holes connecting the nanochannels for fluid supply via micrometer size liquid reservoirs are included. A set of two wafers were combined, the first comprising the nanotrenches and the connecting microtrenches, the second one containing the thin membrane. The two wafers are conjointed by fusion bonding after which the second wafer is completely removed, leaving out only the membrane with the access holes on top of the first wafer (see Fig. 1).

More in detail, a layer of silicon oxide (79 nm) was grown on top of a ⟨100⟩ silicon wafer by dry oxidation. The thickness of this silicon oxide spacer layer determines the thickness of the nanochannels and can be precisely controlled by adjusting the oxidation time. Standard photolithography and 1% HF etching were carried out to transfer the nanochannel pattern. A second photolithography process has been performed to define the supplying microchannels that were subsequently etched by cryogenic plasma. In this step rulers were etched next to nanochannels to be able to measure accurately the position of the moving meniscus (see Fig. 2). The second wafer is processed as follows: a 79 nm thick $SiO_2$ layer was thermally grown. Subsequently, a stoichiometric (high stress) silicon nitride layer of 97 nm thickness was deposited onto the oxidized substrate by low pressure chemical vapor deposition (LPCVD). Access holes for the liquid were patterned on top of the thin film via reactive ion etching (RIE). Before bonding, both wafers were cleaned, first by using a wet chemical $HNO_3$ solution, next in $H_2O_2/H_2SO_4$ (in 1:3; "piranha"), to assure a hydrophilic surface. The piranha solution should be handled with care as it may result in explosion or skin burn if handled incorrectly. In the prebonding "bottom to top alignment" was performed with the Mask Aligner EVG 620. The wafer pair was annealed into a furnace ($N_2$) at 1100 °C for 2 h. Finally, the sacrificial silicon wafer was removed by RIE.

The channel height was measured by means of an ellipsometry measurement of the silicon oxide spacer layer using a Plasmos SD 2002 ellipsometer. The error in the height measurement is estimated to be 3 nm, as a result of the variation in the thickness of the silicon oxide layer on the wafer surface and the precision of the instrument.

## III. MODELING

The filling speed of a liquid in an undeformable capillary can be described by the Washburn model.[10] Washburn considers the capillary pressure due to surface wetting of the inner channel walls as the driving force for liquid transport. This force originates from the pressure drop across the front meniscus, for which the Young-Laplace equation holds.[11] For a flat hydrophilic channel of rectangular cross section (con-

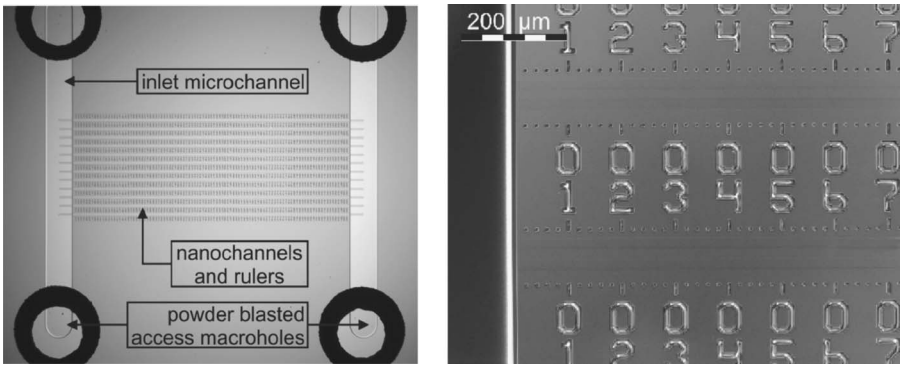


FIG. 2. Left: photograph of a finished chip. Right: close-up microscope image of the nanochannels, the rulers, and the reservoir (Ref. 16) [photographs produced by Haneveld (Ref. 16)].

Downloaded 09 Jul 2007 to 130.89.1.19. Redistribution subject to AIP license or copyright, see http://jap.aip.org/jap/copyright.jsp

stant height $h_0$ and width $w$) with a meniscus having a contact angle $\theta$ with the channel walls, the Laplace pressure becomes

$$p_L = -2\gamma \cos\theta\left(\frac{1}{h_0}+\frac{1}{w}\right), \tag{1}$$

where $p_L = p_{\mathrm{liq}} - p_{\mathrm{vap}}$ is the (Laplace) pressure difference between the liquid side $p_{\mathrm{liq}}$ and the vapor side $p_{\mathrm{vap}}$ of the meniscus, and $\gamma$ is the surface tension of the liquid in air.[30]

If the flow in the channel is fully developed and laminar, the supply of liquid to the moving front can be modeled by a hydraulic resistance, increasing proportional to the length of the liquid plug.[12,31] For a rectangular channel of height $h$ and width $w \gg h$, the averaged velocity $v$ at position $x$ can be calculated as[32]

$$v(x) = -\frac{h^2}{12\eta}\frac{dp(x)}{dx}, \tag{2}$$

with $p$ the local pressure in the fluid and $\eta$ the dynamic viscosity. Writing the pressure drop $dp/dx$ along the fluid column of length $x$ as $p_L/x$, substituting this in Eq. (1) and subsequently integration, gives the extended equation of Washburn, which shows the position of the moving meniscus $x$ as a function of time $t$,

$$x = \sqrt{\frac{\gamma\cos(\theta)h_0^2}{3\eta}\left(\frac{1}{h_0}+\frac{1}{w}\right)t} = a_w\sqrt{t}, \tag{3}$$

with $a_w$ the Washburn constant. In the case of an elastic capillary, the negative pressure in the liquid deforms the channel geometry and the cross section of the channel depends on $x$.

Let us assume that the pressure is constant along the channel width, in the $y$ direction. Moreover, the length of the channel is much larger than the channel width, so that the curvatures in the $x$ direction are much smaller than the curvatures along $y$. Then the $x$ and $y$ directions are actually decoupled and the deflection along the $y$ axis due to the uniform load at given point $x$ obeys for a cross section of intrinsic stress $S$ and flexural rigidity $D$ (per unit length),

$$Dh''''(x,y) - Sh''(x,y) = p(x), \tag{4}$$

where $h'$ stands for $\partial h/\partial y$ and $p(x) = p_{\mathrm{liq}} - p_{\mathrm{air}}$ is the pressure difference between the local pressure inside the fluid and the pressure outside, i.e., across the flexible membrane. With the appropriate boundary conditions this equation is easily solved for $h$.[33,34] We find a maximum deflection at $y=0$ proportional to the applied load, with a proportionality constant $\alpha$ depending on material properties and the shape of the deflection curve.[33,34] Therefore, the local height of the channel can be written as

$$h(x, y=0) = h_0 + \alpha p(x), \tag{5}$$

with $h_0$ the height of the channel at the beginning, at $x=0$. With $Q$ the total volume flow, the fluid velocity $v(x)$ for a channel of height $h$ and width $w$ can be expressed as

$$v(x) = \frac{Q}{hw}. \tag{6}$$

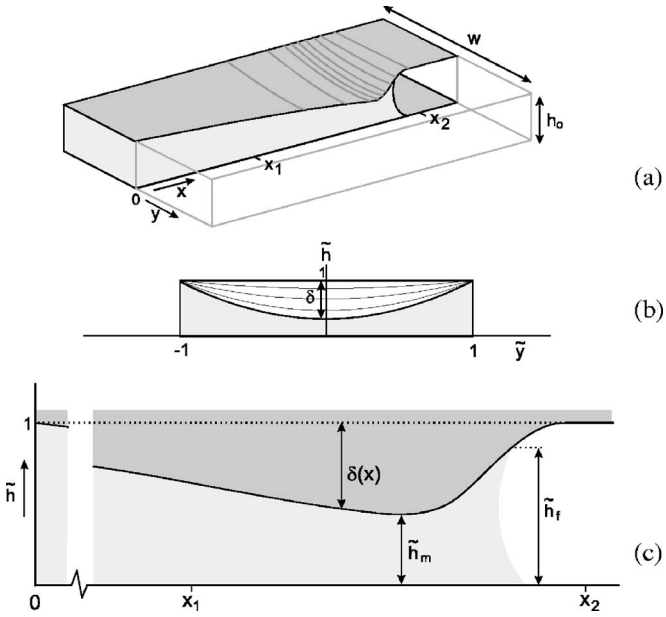


FIG. 3. (a) Model geometry of the channel with definitions of the used variables, with $w$ the channel width, $h_0$ the original channel height, $\delta(x)$ the normalized deflection at the center $y=0$, and $\tilde{h}_m$ and $\tilde{h}_f$ the normalized minimum height and the height at the front (i.e., at the meniscus), respectively. (b) A channel cross section and (c) a longitudinal view.

We can substitute this in Eq. (2) and express the local pressure gradient $dp/dx$ as $(1/\alpha)\partial h/\partial x|_{y=0}$ to obtain a differential equation for $h(x)$. Taking the $y$ dependence of the height $h$ into account and assuming that the flow remains fully developed everywhere along the channel, the equation for $h$ becomes

$$\frac{\partial h(x,y)}{\partial x} = -12\alpha\mu Q\left[\int_{-w/2}^{w/2} h^3(x,y)dy\right]^{-1}. \tag{7}$$

The pressure along the channel width $w$ is constant. Since the deflections are small with respect to $w$, the height $h$ along the $y$ direction can be expanded in $y$. The bending profile $h(x,y)$ is symmetric in $y$ and the approximation up to lowest order in $y$ becomes therefore (with $h=h_0$ at the points $y=\pm w/2$),

$$\tilde{h}(x,y) = 1 + \delta(\tilde{y}^2 - 1), \tag{8}$$

with the normalized variables

$$\delta = \frac{h_0 - \bar{h}(x)}{h_0}, \quad \tilde{h}(x,y) = \frac{h(x,y)}{h_0}, \quad \tilde{y} = \frac{y}{w/2}, \tag{9}$$

in which $\bar{h}(x)$ represents the channel height at $y=0$ (see Fig. 3).

Substitution in Eq. (7) gives, after performing the integration over $y$ only,

Downloaded 09 Jul 2007 to 130.89.1.19. Redistribution subject to AIP license or copyright, see http://jap.aip.org/jap/copyright.jsp

$$\frac{d\bar{h}}{dx} = -12\frac{\mu Q\alpha}{h_0^3 \bar{w}}, \quad \bar{w}(x) = w\left(1 - 2\delta + \frac{8}{5}\delta^2 - \frac{16}{35}\delta^3\right), \tag{10}$$

which can be integrated over $x$ to give an implicit relation between $\bar{h}(x)$ and $x$. Applying the boundary condition that $\bar{h}(x)=h_0$ at $x=0$, this relation becomes

$$x = \frac{w}{12\mu\alpha Q}\left[\frac{44}{105}h_0^4 - \frac{1}{35}\left(5h_0^3\bar{h} + 3h_0^2\bar{h}^2 + \frac{8}{3}h_0\bar{h}^3 + 4\bar{h}^2\right)\right]. \tag{11}$$

To find the velocity of the meniscus at location $x_m$, we have to substitute for $\bar{h}(x)$ in Eq. (11) the minimum height of the channel, $h_m=\bar{h}(x_m)$. The height of the channel where the deflection is largest, $h_m$, is seen to be situated just behind the front meniscus, due to the fact that at the meniscus at the very front of the fluid column, the pressure forces act only on approximately one half of the membrane area. We make therefore the approximation that the deflection of the membrane at the meniscus, is one half the deflection at the height $h_m$ (Ref. 35)

$$h_m = h_0 - 2(h_0 - h_f). \tag{12}$$

The height of the channel at the front meniscus, $h_f$, can then be found by combination of the expression for the pressure [Eq. (1)] and that for $h(x)$ [Eq. (5)], yielding

$$h_f = \frac{h_0}{2} - \frac{\alpha\gamma\cos\theta}{2w} + \sqrt{\left(\frac{h_0}{2} - \frac{\alpha\gamma\cos\theta}{2w}\right)^2 - \alpha\gamma\cos\theta}. \tag{13}$$

Using $Q=wh_f(dx_f/dt)$ and $dx_f \approx dx_m$, one finds for the location $x_m$ of the meniscus as a function of time,

$$x = a_m\sqrt{t}, \tag{14}$$

with $a_m$ the "modified Washburn coefficient,"

$$a_m = h_0^2\sqrt{\frac{1}{6\eta\alpha h_f}\left[\frac{44}{105} - \frac{1}{35}\left(5\tilde{h}_m + 3\tilde{h}_m^2 + \frac{8}{3}\tilde{h}_m^3 + 4\tilde{h}_m^4\right)\right]} \tag{15}$$

and $\tilde{h}_m=h_m/h_0$ with $h_m$ given by Eq. (12).

Let us analyze the value of $a_m$ that we defined as the modified Washburn coefficient [Eqs. (14) and (15)], in comparison to $a_w$, the proportionality constant as defined in Eq. (3). If the bending effects are small, so that $(h_0-h_m)/h_0 \ll 1$, and if we assume further that $w \gg h_0$, we can make a first-order approximation in $\alpha$ for the modified Washburn coefficient and write Eq. (15) as

$$a_m = a_w(1+\varepsilon), \tag{16a}$$

with

$$\varepsilon = -\frac{\alpha\gamma\cos\theta}{h_0}\left(\frac{1}{w} + \frac{1}{h_0}\right). \tag{16b}$$

We see that, for an infinitely stiff membrane ($\alpha \to 0; h_m \to h_0$), $\varepsilon$ approaches zero and we find the original Washburn coefficient again.

For large deflections, however, the value of $a_m$ deviates considerably from $a_w$. Of special interest is the situation when the height $h_m$ decreases to zero—when the membrane almost touches the bottom of the channel. Calculating the corresponding value for $\alpha$ by setting $h_m=0$ in Eqs. (12) and (13), and substituting this value for $\alpha$ in Eq. (15), gives for the modified Washburn coefficient at which $h_m=0$, $a_{m,c}$,

$$a_{m,c} = \sqrt{\frac{44\gamma h_0}{315\eta}\left(\frac{2h_0}{w} + 4\right)} = a_w\sqrt{\frac{44}{105}\left(\frac{2h_0}{w} + 4\right)}. \tag{17}$$

Assuming $h_0/w \ll 1$, it is seen that $a_{m,c} \approx 1.29a_w$. Just before the upper membrane bends so much down that it touches the bottom ($h_m \to 0$), the modified Washburn coefficient is about 29% larger than the original Washburn coefficient.

Qualitatively, the membrane bending due to the induced negative pressure in the liquid does not alter the square root of time dependence of $x(t)$, but quantitatively, the filling speed is up to 29% higher than in an undeformed channel.

The smaller channel height $h_f$ at the front end of the fluid column implies a larger pressure drop across the meniscus, thereby increasing the filling speed. Conversely, the hydraulic resistance along the channel is increased due to the lower height, which has a negative influence on the velocity. For small deflections (small $\alpha$) the latter effect dominates and the velocity is slightly lower than the normal Washburn speed; this is illustrated by the fact that $\varepsilon$ is negative. For large deflections, an increased filling speed results.

## IV. EXPERIMENTS

To investigate these effects we performed filling experiments on the channels of different widths that were fabricated as described previously. The wider channels will have a lower mechanical stiffness, corresponding to a higher $\alpha$ [Eq. (5)], so that the capping layer will bend more. On the other hand, the pressure drop due to the horizontal curvature decreases with increasing width. The value of $\alpha$ as calculated from the mechanical model[33] ($\alpha \sim f(w)w^4$) shows that $\alpha$ strongly increases with the width. Using this expression, the constant $a_m$ was calculated for given channel height and fluid properties as a function of the channel width.

In the experiments, we investigated the filling of different liquids, water, ethanol, cyclohexane, and acetone, in channel arrays. A channel array consists of 17 parallel channels and has a length of about 10 mm. The individual channels in an array have a height of 79 nm and a width varying from 2.5 to 10.6 $\mu$m. The experiments were performed under constant temperature, measured to be 21.2±0.5 °C. To measure the position of the meniscus as a function of time, a droplet of liquid was introduced into the access holes by pipetting so that the array of nanochannels could fill by capillary action. As the channels filled, we were able to observe a change in contrast and color due to the difference between the refractive index of liquid and the refractive index of the air in the vacant channels. Each filling experiment was performed in a fresh channel to avoid any contamination. The

Downloaded 09 Jul 2007 to 130.89.1.19. Redistribution subject to AIP license or copyright, see http://jap.aip.org/jap/copyright.jsp

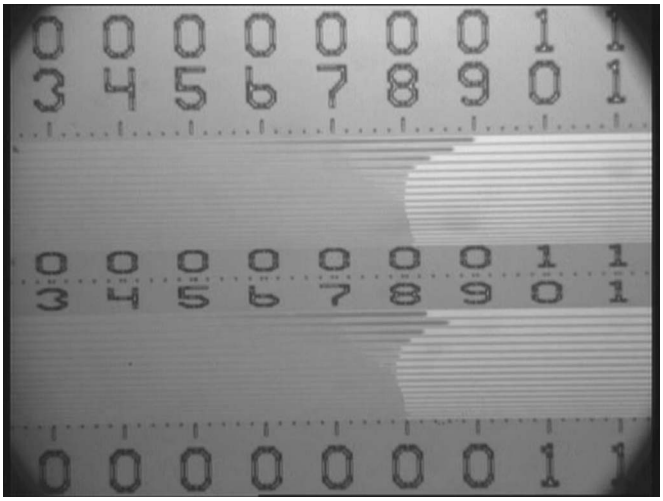

FIG. 4. A typical still image of the capillary filling of nanochannels (ethanol) of various widths, varying from $w=2.5$ to 10.5 $\mu$m. The large thicks represent a distance of 100 $\mu$m.

channels were observed under an upright microscope (Leica LM/DM) in bright field mode. Mitutoyo 20× objective numerical aperture (NA)=0.28 was used. The filling process was recorded by video imaging with a frame rate of 25 images/s, and the position of the meniscus as a function of time was measured by means of frame by frame analysis of the recorded videos. We concentrated on the first 40 s of these videos, corresponding to a fluid column length in the order of several millimeters, during which a sufficient fluid supply was ascertained. Figure 4 shows a typical still image from the video capture of the filling of nanochannels. Analysis of the position $x$ as a function of $t^{1/2}$ showed a quite good linear relation, see Fig. 5 for some representative curves, so that the slope $a$ of $x$ vs $t^{1/2}$ could be determined accurately.

In Fig. 6 the thus determined slope $a$ for the filling process in channels of different widths is depicted. Four different liquids are reported. Also plotted are the theoretic curves of $a_m$ according to Eq. (15) as a function of the channel

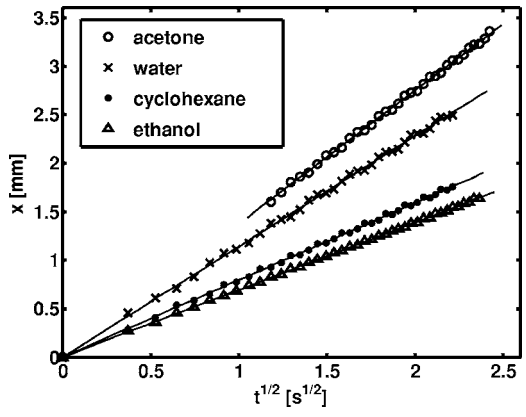


FIG. 5. Measured position $x$ of the moving meniscus vs the square root of the filling time, for four liquids in different channels with a channel height $h_0=79$ nm. (For the depicted curve of water, the channel width was $w=6.0\pm0.4$ $\mu$m; for ethanol, cyclohexane, and acetone, $w=9.0\pm0.4$ $\mu$m. These widths correspond to a deflection of $h_m=h_0/2$.) These measurements were carried out at a temperature of (21.2±0.5 °C). The error in the measured position is about 20 $\mu$m, the error in $t^{1/2}$ is 0.03 $s^{1/2}$. The relation between $x$ and $t^{1/2}$ is in very good approximation linear.

width. In calculating the value of $a_m$ for the four liquids, we inserted the dynamic contact angle $\theta_d$, that was zero for ethanol, acetone, and cyclohexane because of the complete wetting of these liquids, and a value $\theta_d<5°$ for water on $SiO_2$ and $\theta_d=12°$ for water on SiN, as was measured using the Krüss contact angle measurement system G 10, and the data processed with the program DROP SHAPE ANALYSIS 1.51. The good linear fit with the $x\sim t^{1/2}$ scaling law in Fig. 5 implied that the dynamic contact angle remained independent from velocity for the time scale of the experiments. This velocity independence of the contact angle is in correspondence with results obtained by Sobolev *et al.*[9] The curves in Fig. 6 show clearly the deviation of $a_m$ from the normal Washburn coefficient $a_w$ at relatively large channel widths, due to the larger deflections of the membrane for the wider channels.

We see in Fig. 6(c) (for water) that for channel widths above approximately 8 $\mu$m the experimental results lie below the theoretical curve. This deviation can be attributed to the fact that the membranes of those channels that are close to complete collapse, incidentally stick to the bottom of the channels. The incidental complete collapses reduce the effective filling speed and the model loses its validity in these cases. The channel width at which complete collapse occurs is the smallest for water, since this liquid has the highest surface tension of the four investigated liquids.

For small channel widths, corresponding to small membrane deflections, the experimentally determined value of $a_m$ agrees well with the theoretic curve and cannot be distinguished, within the experimental error, from the normal Washburn coefficient $a_w$. As analyzed by Ransohoff and Radke,[36] Dong and Chatzis,[37] and Weislogel and Lichter,[38] the wetting liquid in front of the meniscus will imbibe in the corners of the square capillary channel and therefore our results imply also that this corner flow has no measurable influence on the velocity of the main meniscus.

Analysis of the video images of the filling on a small time resolution of 0.04 s shows that the wider channels exhibit a typical filling behavior—the fluid fills irregularly by starts and stops. This unsteady filling is observed for channels that are close to complete collapse, with a width that is larger than 6–8 $\mu$m, depending on the precise fluid parameters. The exact nature of this phenomenon is currently under investigation and out of the scope of the present paper. On the longer time scale of several seconds, these irregularities are averaged out, as Fig. 5 illustrates, and the filling follows well a $x\sim t^{1/2}$ scaling law.

With Eq. (15) and the implicit dependence of $h_m$ and $h_f$ on the normalized deflection $\delta$ [Eqs. (9) and (12)], it is also possible to obtain the modified Washburn coefficient $a_m$ as a function of the deflection $\delta$ of the membrane. By normalizing $a_w$ and $a_m$ by $a_0=\sqrt{\gamma h_0 \cos\vartheta/3\eta}$ the result becomes independent of fluid parameters. Figure 7 shows both $a_w$ and $a_m$ as a function of the deflection $\delta_{\max}$, where $\delta_{\max}$ is defined as $\delta_{\max}=1-\tilde{h}_m$ (i.e., the deflection at the point of minimal height $h_m$ of the membrane, see Fig. 3) The dependence of $a_m$ in Eq. (3) on $\delta_{\max}$ is a result of the fact that $\delta_{\max}$ depends on the stiffness of the membrane, characterized by the parameter $\alpha$, that is strongly dependent on the channel width. Measurement results of all four liquids are represented in

Downloaded 09 Jul 2007 to 130.89.1.19. Redistribution subject to AIP license or copyright, see http://jap.aip.org/jap/copyright.jsp

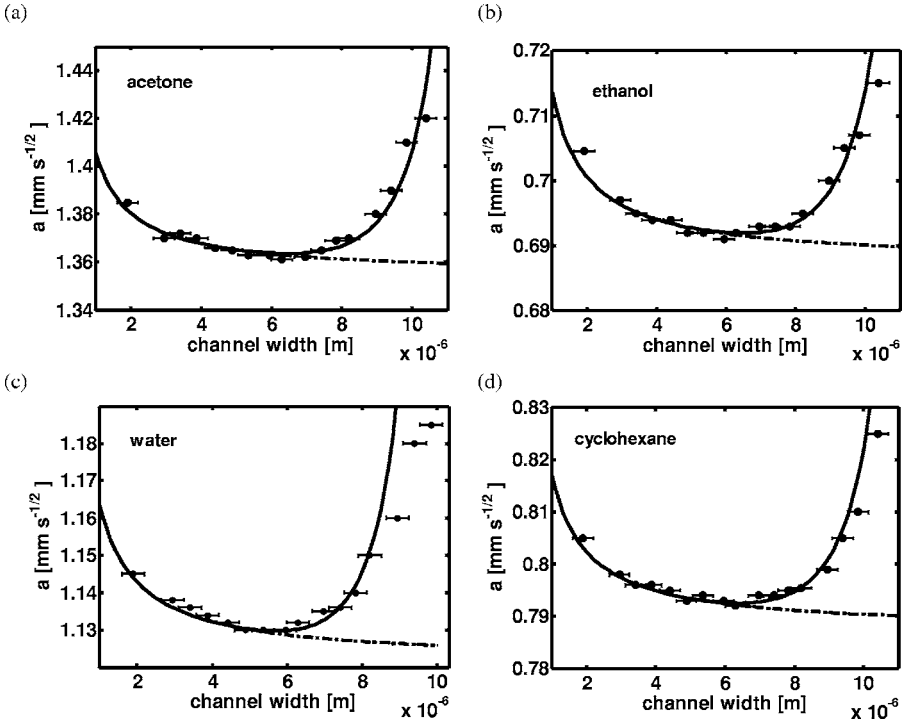


FIG. 6. Experimentally determined slope $a$ of $x=at^{1/2}$ for different channel widths. The dashed line depicts the value of $a_w$ that follows from the original Washburn relation, and the solid line represents $a_m$ according to Eq. (15). Four different liquids are depicted.

Fig. 7. The inset of the figure shows the full scale $0<\delta_{\max}<1$ showing that at $\delta_{\max}=1$, $a_m\approx 1.29a_w$ as noted before—at almost complete deflection of the membrane down to the bottom, the model predicts an increase of the filling speed by approximately 29%.

The recorded video results permit in particular the analysis of channels for which $h_m=h_0/2$.

Setting $h_m=h_0/2$ in Eqs. (12) and (13), solving for $\alpha$ and substituting $\alpha$ in Eq. (15) gives for the modified Washburn coefficient at $h_m=h_0/2$,

$$a_m = a_w\sqrt{\frac{2080}{1890}\left(\frac{3h_0}{4w}+1\right)}, \quad h_m = h_0/2, \tag{18}$$

which is, for $h_0/w\ll 1$, $a_m^2\approx 1.10a_w^2$, or $a_m\approx 1.05a_w$. At this value of $\alpha$, the corresponding width can be calculated for the four different liquids and the filling behavior analyzed. We can thus obtain the value of $a_m$ as a function of the relevant parameter in this case, $\gamma/\eta$, the capillary velocity. The result is shown in Fig. 8, where the drawn line depicts the curve of $a_m^2$ according to Eq. (18), and the dotted line the square of the normal Washburn coefficient $a_w^2$. A good agreement is seen between the experimentally determined filling speeds for these liquids and the values following from the model.

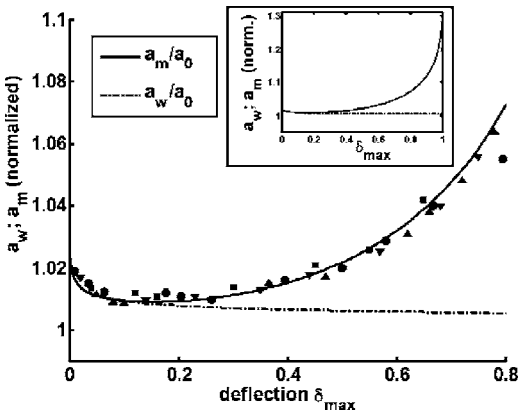


FIG. 7. The modified Washburn coefficient $a_m$ according to Eq. (15) and the Washburn coefficient $a_w$ as a function of the normalized maximal deflection of the membrane $\delta_{\max}=1-\tilde{h}_m$. Both $a_m$ and $a_w$ have been normalized by $a_0=\sqrt{\gamma h_0\cos\vartheta/3\eta}$, so that four different liquids can be depicted in one figure. The inset shows the full scale $0<\delta_{\max}<1$, with $\delta_{\max}=1$ and $a_m\approx 1.29a_w$. The symbol ● represents measurements on water; ■ shows ethanol; ▲: acetone, and ▼: cyclohexane.

## V. CONCLUSIONS

In this paper we studied the filling kinetics of nanochannels with varying cross sections due to the deforming capping layers and found that the filling speed of all investigated liquids in the nanochannels is significantly altered by the deformation of the thin channel membranes. It is observed that the filling behavior still follows qualitatively the $x\sim t^{1/2}$ scaling law. This is to some extent remarkable, since two different effects related to the channnel deformation

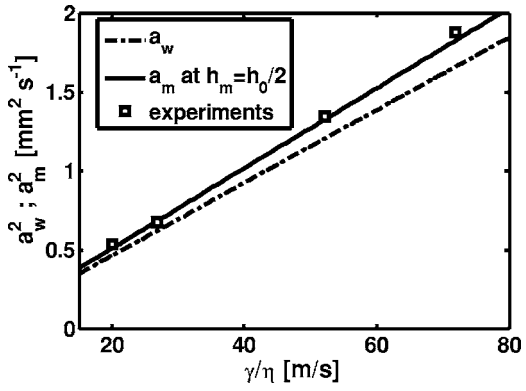


FIG. 8. Experimentally determined slope $a$ of $x=at^{1/2}$ for different liquids as a function of the capillary velocity $\gamma/\eta$. The dashed line shows $a_w^2$, the calculated coefficient $a_m^2$ at $h_m=h_0/2$, according to Eq. (18) is given by the solid line.

Downloaded 09 Jul 2007 to 130.89.1.19. Redistribution subject to AIP license or copyright, see http://jap.aip.org/jap/copyright.jsp

compete: on the one hand the flow resistance increases drastically due to the smaller cross section, whereas on the other hand the Laplace pressure becomes more negative as a consequence of the increased meniscus curvature.

A model describing this dynamic elastocapillary effect was presented. Measurements on the filling speed of four liquids of varying viscosity and surface tension in channels of varying widths and therefore with different membrane deflections permitted the verification of the model. For extreme bending of the capping layers, down to the channel bottom, an increase of the filling speed by 29% compared with the conventional Washburn speed for undeformed rectangular channels is theoretically predicted. For deflections of the flexible membranes of up to approximately 0.8 times the original channel height, the proposed model could be experimentally verified and is seen to describe accurately the experimental results both qualitatively and quantitatively.

## ACKNOWLEDGMENTS

The authors thank the Dutch Technology Foundation STW for financial support and are also grateful to Ruud Spiering and Theo Lammerink for their fruitful contributions.

[1]M. G. Stern, M. W. Geis, and J. E. Curtin, J. Vac. Sci. Technol. B **15**, 2887 (1997).
[2]J. Han and H. G. Craighead, Science **288**, 1026 (2000).
[3]M. Foquet, J. Korlach, W. Zipfel, W. W. Webb, and H. G. Craighead, Anal. Chem. **74**, 1415 (2002).
[4]H. Cao, Z. Yu, J. Wang, J. O. Tegenfeldt, R. H. Austin, E. Chen, W. Wu, and S. Y. Chou, Appl. Phys. Lett. **81**, 174 (2002).
[5]N. R. Tas, J. W. Berenschot, P. Mela, H. V. Jansen, M. Elwenspoek, and A. Van den Berg, Nano Lett. **2**, 1031 (2002).
[6]J. Haneveld, H. V. Jansen, J. W. Berenschot, N. R. Tas, and M. Elwenspoek, J. Micromech. Microeng. **13**, S62 (2003).
[7]L. Mercury and Y. Tardy, Geochim. Cosmochim. Acta **65**, 3391 (2001).
[8]N. R. Tas, P. Mela, T. Kramer, J. W. Berenschot, and A. Van den Berg, Nano Lett. **3**, 1537 (2003).
[9]V. D. Sobolev, N. V. Churaev, M. G. Velarde, and Z. M. Zorin, J. Colloid Interface Sci. **222**, 51 (2000).
[10]L.-J. Yang, T.-J. Yao, and Y.-C. Tai, J. Micromech. Microeng. **14**, 220 (2004).
[11]E. W. Washburn, Phys. Rev. **17**, 273 (1921).
[12]N. R. Tas, J. Haneveld, H. V. Jansen, M. Elwenspoek, and A. Van den Berg, Appl. Phys. Lett. **85**, 15 (2004).
[13]N. V. Churaev, V. D. Sobolev, and Z. M. Zorin, *Special Discussion on Thin Liquid Films and Boundary Layers* (Academic, New York, 1971), pp. 213–220.
[14]A. Hibara, T. Saito, H.-B. Kim, M. Tokeshi, T. Ooi, M. Nakao, and T. Kitamori, Anal. Chem. **74**, 6170 (2002).
[15]A. Han, G. Mondin, N. G. Hegelbach, N. F. de Rooij, and U. Staufer, J. Colloid Interface Sci. **293**, 151 (2006).
[16]J. Haneveld, Ph.D. thesis, University of Twente, 2006.
[17]T. Eisner and D. J. Aneshansley, Proc. Natl. Acad. Sci. U.S.A. **97**, 6568 (2000).
[18]A. K. Geim, S. V. Dubonos, I. V. Grigorieva, and K. S. Novoselov, Nat. Mater. **2**, 461 (2003).
[19]T. Tanaka, M. Morigami, and N. Atoda, Jpn. J. Appl. Phys., Part 1 **32**, 6059 (1993).
[20]C. H. Mastrangelo and C. H. Hsu, J. Microelectromech. Syst. **2**, 33 (1993).
[21]C. H. Mastrangelo and C. H. Hsu, J. Microelectromech. Syst. **2**, 44 (1993).
[22]N. R. Tas, T. Sonnenberg, H. V. Jansen, R. Legtenberg, and M. Elwenspoek, J. Micromech. Microeng. **6**, 385 (1996).
[23]R. Maboudian and R. T. Howe, J. Vac. Sci. Technol. B **15**, 1 (1996).
[24]C. Y. Hui, A. Jagota, Y. Y. Lin, and E. J. Kramer, Langmuir **18**, 1394 (2002).
[25]K. K. S. Lau, J. Bico, K. B. K. Teo, M. Chhowalla, G. A. J. Amaratunga, W. I. Milne, G. H. McKinley, and K. K. Gleason, Nano Lett. **3**, 1701 (2003).
[26]N. Chakrapani, B. Wei, A. Carrillo, P. M. Ajayan, and R. S. Kane, Proc. Natl. Acad. Sci. U.S.A. **101**, 4009 (2004).
[27]C. Py, L. Doppler, J. Bico, B. Roman, P. Reverdy, and C. N. Baroud, American Physical Society, 59th Annual Meeting of the APS Division of Fluid Dynamics, November 19–21, 2006.
[28]H.-Y. Kim and L. Mahadevan, J. Fluid Mech. **548**, 141 (2006).
[29]J. Bico, B. Roman, L. Moulin, and A. Boudaoud, Nature (London) **432**, 690 (2004).
[30]R. J. Hunter, *Foundations of Colloid Science*, 2nd ed. (Oxford University Press, Oxford, 2001), pp. 53–55.
[31]T. S. J. Lammerink, N. R. Tas, J. W. Berenschot, M. Elwenspoek, and J. H. J. Fluitman, Proceedings of the IEEE Micro Electro Mechanical Systems 1995 Conference, Amsterdam, The Netherlands, 1995, pp. 13–18.
[32]L. D. Landau and E. M. Lifschitz, *Fluid Mechanics*, Course of Theoretical Physics Vol. 6, 2nd ed. (Butterworth and Heinemann (Elsevier Sci. Lim.), Oxford 2003).
[33]The bending stiffness for cylindrical bending of a membrane under a uniform pressure load $p$, including the effect of an intrinsic stress in the membrane, is for example given by Timoshenko and Woinowsky-Krieger (Ref. 34). In a simple representation the compliance is given by $\alpha = \delta(u,p)/p = (\zeta^4/D)f(u)$, where $\delta$ is the center deflection, $D$ is the flexural rigidity of the composite membrane, $\zeta$ is half the channel width, $f(u)^{-1}$ is the stiffening due to the presence of the intrinsic stress as a function of the dimensionless parameter $u = w(\Sigma\sigma_i t_i/D)^{1/2}$, with $\sigma_i$ and $t_i$ the stress and the thickness of layer $i$, respectively, and $f(u) = (1/u^4)(u^2/2 + u/\sinh u - u/\tanh u)$.
[34]S. P. Timoshenko and S. Woinowsky-Krieger, *Theory of Plates and Shells* (McGraw-Hill, New York, 1959), Chap. 1.
[35]The factor of one half is only a motivated estimation, based on the physical argument presented in the text. Analysis of the influence of the precise value of this factor in the subsequent derivation shows only a small quantitative and no qualitative change of the final result. Taking in Eq. (12) instead of the factor 2 the more general parameter $\kappa$, and calculating $d(a_m^2)/d\kappa$ around $\kappa=2$, one finds $da_m^2/d\kappa \approx 0.02a_m^2$: a change in $\kappa$ of $\Delta\kappa$ near $\kappa=2$ leads to a relative variation in $a_m^2$ of $(\Delta a_m^2)/a_m^2 \approx 0.02\Delta\kappa$.
[36]T. C. Ransohoff and C. J. Radke, J. Colloid Interface Sci. **121**, 392 (1988).
[37]M. Dong and I. Chatzis, J. Colloid Interface Sci. **172**, 278 (1995).
[38]M. M. Weislogel and S. Lichter, J. Fluid Mech. **373**, 349 (1998).

**Downloaded 09 Jul 2007 to 130.89.1.19. Redistribution subject to AIP license or copyright, see http://jap.aip.org/jap/copyright.jsp**